Journal of Cultural Heritage 74 (2025) 322–331

Contents lists available at ScienceDirect

Journal of Cultural Heritage

journal homepage: www.elsevier.com/locate/culher

Original article

Reviving the colors of paintings by removing the protective coating: a physical and virtual intervention

José A.R. Monteiro[a,*], Liliana Cardeira[b], Ana Bailão[b], Sérgio Miguel Cardoso Nascimento[a], João M.M. Linhares[a]

[a] Physics Center of Minho and Porto Universities (CF-UM-UP), Gualtar Campus, University of Minho, 4710-057 Braga, Portugal
[b] Universidade de Lisboa, Faculdade de Belas-Artes, Centro de Investigação e de Estudos em Belas-Artes (CIEBA), Largo da Academia Nacional de Belas-Artes, 1249-058 Lisboa, Portugal

ARTICLE INFO

Article history:
Received 18 July 2024
Accepted 23 June 2025

Keywords:
Hyperspectral image
Conservation and restoration
Digital restoration
Varnish aging
Neural networks
Kubelka-Munk theory

ABSTRACT

When an existing coating over a painting is detrimental to its reading and full appreciation, it needs to be removed. Coating removal to reveal the underlying painting, with minimal physical intervention, may provide additional information regarding the painting and guidance for its restoration or intervention.
A Neural Network (NN) was devised to simulate the removal of a painting's coating, using as training data a small area of the painting where the coating had been physically removed. Simulations of coating removal using the NN and two additional methodologies were compared to actual physical removal.
Hyperspectral images of the paintings with and without coating were acquired, and chromatic variations were computed by estimating differences in just-noticeable different colors (JND) values and in the color gamut, using CIECAM16-UCS. Comparisons were made between paintings with and without coating, and between paintings without coating and their simulations.
Results showed that removing the coating led to an increase in JND values (1.8 times on average) and in the color gamut, but the magnitude was dependent on the initial condition of the coating. When simulating coating removal, the NN produced the best chromatic simulation, with an average JND of approximately 2.6 ± 0.5 (1.1 ± 0.2 excluding lightness), while other methodologies produced differences of approximately 8.6 ± 5.7 (3.7 ± 3.0 excluding lightness).
Results achieved with the NN highlight its capability for simulating coating removal with minimal physical intervention to the painting, a valuable tool when complete coating removal without outcome prediction would be undesirable.

1. Introduction

The protective varnish layer (coating) applied to paintings serves two main purposes: to protect the painting's surface from external agents, e.g. water and dust, and to enhance its appearance by increasing its color saturation and contrast [1–4]. The perceptual improvement is due to the interaction of light with the painting's surface, particularly the multiple reflections at the air/varnish/paint interfaces [3,5,6], the molecular weight of the coating and the texture of the painting surface (binder and pigment) [7]. Over time, the coating deteriorates, becoming yellowish and darker, losing gloss and elasticity, and developing cracks, imposing transmittance and structural changes on the painting [5,8–10]. These changes to the coating are caused by an oxidation process driven by external agents present in the environment, such as natural and artificial light and humidity. This aging process impacts the visual reading of the painting, by changing the transmittance of the interfaces [5,11], a change that may not be uniform across the painting's surface.

The physical removal of an aging coating will expose the colors underneath and improve the reading of the painting, a task that falls under the regular work of a painting conservator. Nevertheless, previewing the color changes before the actual intervention would provide valuable information to the painting conservator and the owner, as the result may differ greatly from the existing reading of the painting [12].

* Corresponding author.
E-mail addresses: alexmonteiro1995@gmail.com (J.A.R. Monteiro), lilianacardeira@gmail.com (L. Cardeira), ana.bailao@edu.ulisboa.com (A. Bailão), smcn@fisica.uminho.pt (S.M.C. Nascimento), jlinhares@fisica.uminho.pt (J.M.M. Linhares).

https://doi.org/10.1016/j.culher.2025.06.015

Previous works simulated the removal of the coating to support the restoration process [5,9,11,13–15], by collecting the spectral properties of the painting and the coating through localized measurements of the coating's transmittance using low or point-based spatial resolution instruments, such as direct spectrophotometers [16]. Localized measurements of the painting's spectral properties require extrapolating the locally obtained information to the entire painting, disregarding spatial variations in the oxidation process or the uniformity of the coating [17]. Other works used multispectral imaging systems capable of imaging the whole painting, but with low spectral resolutions [8,14,18]. Chemical analyses may also be used to estimate the composition of the coating and directly measure, or infer, its transmittance, but implying retrieving a localized physical sample of the coating from a hidden area of the painting and extrapolating it globally, again disregarding the coating's spatial variations [19,20]. Such a methodology has the advantage of keeping the visible portion of the painting intact but will require a physical sample and direct intervention on the painting. Theoretical approaches, as the Kubelka-Munk two-constant theory, have attempted to model the optical properties of the coating with minimal to no physical interaction with the painting. This mathematical model accurately describes the interactions between light and transparent or translucent materials, particularly the internal reflections at the coating level in paintings. It establishes a relationship between the reflectance of the painting with and without varnish, assuming that only light that propagates perpendicular to the surface of the coating is considered, and assuming absorption and scattering in both the incidence and reflected directions of the light [3,5,6,15,21–24]. Developing neural networks (NN) to simulate the removal of the coating requires images of paintings with and without the coating (localized or across the whole painting, making obsolete the simulation process if the whole painting is considered) to be used as reference images to train the NN. Sequential NN are commonly employed to learn patterns or tasks from databases, and generate predictions [25], consisting of sequential layers characterized by several nodes and activation functions. Activation function evaluates the input at each node and weights it to produce a prediction as close as possible to the expected result defined during the training process [26], achieved by adjusting the NN weights of each node iteratively, over a specific number of cycles (or epochs) [27]. Additionally, the NN may use optimizer functions to accelerate the training process, attempting to minimize the error between the prediction and the result [28]. Convolutional NN (CNNs) represent another class of NN that use images as input, characterized by convolutional and max-pooling layers to reduce the dimensionality of the input image, followed by a structure similar to a sequential NN [29–34]. However, it is important to note that reducing the image dimensionality leads to an inevitable loss of the image's original information.

Predicting a painting's appearance beneath its surface coating can assist conservation planning. Such predictions inform treatment strategies and facilitate clear communication with clients by allowing them to visualize possible outcomes before any intervention. Additionally, predictive digital simulation of varnish removal provides a valuable alternative when physical cleaning is not possible. This may be due to the instability of paint layers, the presence of sensitive materials, solubility issues, or ethical considerations related to preserving historic coatings. In these situations, non-invasive visualization techniques offer a practical means for documentation and interpretation, supporting decision-making while minimizing risks to the artwork.

While these predictive tools can help the painting conservator, it is important to recognize the inherent complexities and uncertainties of varnish removal. Removing or replacing a painting's coating is a complex process, with results that are difficult to anticipate. An experienced painting conservator may attempt to estimate the outcome obtaining known information about the painting, such as the artist, creation period, pigments and binders used, or the type of coating. Although examining localized regions where the original paint is exposed can offer valuable reference points, such evidence is often fragmentary and may not provide a comprehensive basis for reconstructing the painting's authentic chromatic scheme. The accuracy of any simulation predicting the effects of removing a painting's coating is limited by several unknown factors including the coating's composition, thickness, distribution, and degradation state. Furthermore, over time, a painting's pigments and/or binder may degrade due to chemical reactions, light exposure, pollutants, microorganisms, or physical damage, resulting in different hues or, occasionally, the formation of new pigments. As such, knowing the coating's composition is insufficient to estimate the painting's underlying colors. The degree of yellowing and other optical changes can vary significantly depending on factors as the coating's thickness, application method, environmental exposure, and degradation state, even when the same material is used.

These unknows limit the predictions of computational models based on coating transmittance but drive the development of more computational models capable of providing visual simulations of the painting's post-intervention appearance [5,7,8,15,35–37].

This work presents and assesses three methodologies capable of simulating the removal of a painting's coating to reveal the underlying colors and spectral data, resorting to hyperspectral images of paintings acquired before and after the physical removal of the coating [14,18,36,38–44]. The methodologies were assessed by colorimetrically comparing the colors obtained with the virtual and with the real removal of the painting's coating.

2. Research aim

The purpose of this study was to evaluate three methodologies for the virtual removal of a painting's coating, with the aim of identifying the most effective approach by analyzing the chromatic changes between the virtual and the actual removal.

3. Material and methods

3.1. Paintings

Fig. 1 represents a painting used in this study, before and after the physical removal of the coating, structural intervention, and restoration for preservation and consolidation of the painting. Named "*Nuno Álvares em Valverde*", from the year 1904, with a size of 46 (H) x 55(V) cm. Table 1 and Fig. 1 in the Supplementary Materials shows the data for all the paintings used.

3.2. The external layer: the coating

The external layer of the paintings was not a uniform, homogeneous coating. Instead, the surfaces displayed irregular applications of coating, intermixed with non-uniform accumulations of dirt and dust, and, in some areas, complete absence of coating. These variations resulted in regions with differing coating thicknesses, localized dirt and dust deposits, and uncoated sections covered solely by particulate matter. The coating removal showed an underlying dirt layer, indicating that the paintings were exposed to environmental conditions before coating application and without prior surface cleaning.

As the outermost layer, the coating was exposed to various deteriorating agents including dirt, fluctuating ambient conditions, ultraviolet radiation, and inappropriate relative humidity and temperature conditions [45]. Prolonged exposure to these factors

Fig. 1. Painting 1 (Nuno Álvares em Valverde) before (a) and after (b) removing the coating and structural.intervention.

typically causes increased rigidity and yellowing of the coating [1–3,11]. The paintings analyzed in this study exhibited coatings with a wide range of degradation and coverage, from entirely absent to highly irregular. Areas with thicker coating appeared darker or more yellowed compared to other portions of the painting, which compromised the readability of the pictorial composition when using HIS [13].

3.3. Cleaning

As there was no information about the type, concentration, or composition of the varnishes used, the paintings' protection and integrity during cleaning was ensured by removing the aged varnish starting with low polarity solutions. The most effective mixture in removing the coating provided clues about the composition of the coating and possible identification of its type, probably a resin of natural origin. A similar process was employed in all paintings until an appropriate solvent was identified as effective on removing the coating, as there were no guarantees that all paintings had the same coating. Further discussion of this process can be found elsewhere [17].

The removal of the coating uncovered a secondary layer of dirt indicating that the paintings were exposed to the environment before being varnished, with the coating subsequently applied over the dirt layer without prior cleaning. The records about each painting did not mention the period during which the paintings were left unvarnished, leaving it unknown.

After assessing and analyzing the layer of dirt, it was removed with a solution of demineralized water and 1 % polyethoxylated lauryl alcohol, Brij® 35, a nonionic surfactant with a neutral pH [46]. Only after the removal of the varnish and the dirt layers, the painting was considered ready for imaging. Further details about the complex cleaning methodology used to ensure extensive coating cleaning may be found in the Supplementary Materials section.

3.4. Hyperspectral images acquisition and processing

Paintings were imaged by a HIS, before and after the removal of the coating and painting cleaning as described elsewhere [17,18,41,42,47,48]. The HIS used was composed of a low-noise Peltier-cooled digital camera with 1344×1024 pixels and a 12-bit digital signal output (Hamamatsu, C4742–80–12AG, Hamamatsu Photonics K.K., Hamamatsu City, Japan) coupled to a fast-tunable liquid-crystal filter (VariSpec, model VS-VIS2–10HC-35-SQ, Cambridge Research & Instrumentation, Inc., MA), mounted in front of a zoom lens working at 75 mm, adjusted to f/11, and controlled by a MatLab in-house developed software (MatLab R2022b, MathWorks, Natick, MA, USA). An infrared filter was positioned in front of the HIS to prevent contamination from out-of-band transmissions of high wavelengths, when tuned to lower wavelengths. The spectral radiance from 400 to 720 nm in 10 nm increments was collected using as light source a discharge lamp (OSRAM HQI 150 W RX7s) with a maximum illuminance of 2000 lx across all areas of the painting to preserve its integrity. Non-uniformities in the illumination field were compensated by imaging a uniform flat surface. The spectral reflectance was estimated from the data acquired considering a surface with known reflectance (Munsell N7, VeriVide Limited, Leicester United Kingdom), imaged with the painting [18,39,49–51].

The HIS image acquisition of the same painting at different times returned images with different sizes and subtle spatial differences because of sequential acquisitions (changes in lighting, camera, and painting position, although minimized) and chromatic aberrations of the system, respectively. To correct for such differences, two image registration procedures were used: one registering the images across wavelengths [51] using as reference the image at 550 nm for its best signal-to-noise ratio, and the other registering across the spatial distortions using the MatLab function *imregtform* [52], resulting in images with comparable pixel information.

3.5. Virtual coating removal

Three virtual coating removal methodologies based on hyperspectral images of paintings were implemented, tested, and compared to identify the most effective method for simulating coating removal on the hyperspectral domain.

3.5.1. Coating removal method 1: average protective layer

The removal of the coating was simulated by assuming Eq. (1)., where the $\boldsymbol{R}_{\boldsymbol{P}_{COATING}}(\boldsymbol{\lambda})$, and the $\boldsymbol{R}_{\boldsymbol{P}_{\boldsymbol{n}COATING}}(\boldsymbol{\lambda})$ represent the reflectance of the painting with and without the coating respectively, while $\alpha(\lambda)$, represents the effect of the coating. Some of the paintings used had undergone reintegration processes, including areas that were repainted, physically reconstructed, or rebuilt. This study did not consider such areas.

$$\boldsymbol{R}_{\boldsymbol{P}_{COATING}}(\boldsymbol{\lambda}) = \boldsymbol{\alpha}(\boldsymbol{\lambda}) \times \boldsymbol{R}_{\boldsymbol{P}_{\boldsymbol{n}COATING}}(\boldsymbol{\lambda}) \quad (1)$$

Estimating $\alpha(\lambda)$ pixelwise for each painting's individual area would compensate for the coating's non-uniformities. However, fulfilling such a requirement would imply knowing the reflectance spectra of the entire painting without the coating, eliminating the need for digital simulation. $\alpha(\lambda)$ was estimated over a limited section of the painting only and assumed to be representative of the

Fig. 2. The W30 area used in the computations, delimited by the red lines, on a sRGB rendering of Painting 1 with the original coating, considering the D65 standard illuminant.

entire coating. A 30-pixel width area (W30) along the periphery of the paintings was used, as represented between the red lines in Fig. 2. The W30 area represents approximately 2 cm measured from the edge of the painting to the red line, an area usually hidden by the painting's frame. The rationale behind this approach was that removing the coating from a hidden area would require minimal visible intervention from the conservator and would not compromise the painting's integrity or appearance if the restoration were not to be completed.

Removing the coating from a surrounding area of the painting, rather than just a localized section, enabled better characterization of the coating's non-uniformities or spatial variations while providing access to a broader gamut of colors for analysis.

$\alpha(\lambda)$ was estimated by using Eq. (2) for each pixel over the W30 area of the hyperspectral image with pixel coordinates (x,y), then averaged across pixels ($\bar{\alpha}(\lambda)_{W30}$) and assumed to be representative of all $\alpha(\lambda)$ values. The virtual simulation of the hyperspectral image of the painting without coating, $R_{P_{S1}(x,y)}(\lambda)$ was then simulated by using Eq. (3).

$$\alpha(\lambda)_{(x,y)} = \frac{R_{P_{COATING}(x,y)}(\lambda)}{R_{P_{nCOATING}(x,y)}(\lambda)} \tag{2}$$

$$R_{P_{S1}(x,y)}(\lambda) = \frac{R_{P_{COATING}(x,y)}(\lambda)}{\bar{\alpha}(\lambda)_{W30}} \tag{3}$$

3.5.2. Coating removal method 2: Kubelka-Munk two-constant theory

The Kubelka-Munk two-constant theory described elsewhere [1,5,6,21–23,53] was used assuming the $R_{P_{nCOATING}(x,y)}(\lambda)$, computed using Eq. (4), the body reflection of the coating ($R_V^b(\lambda)$), the reflectance of the painting substrate ($R_P^b(\lambda)$), and the transmittance of the coating ($T(\lambda)$) estimated using Eq. (5) [5,23].

The virtual simulation of a hyperspectral image of the painting without coating, $R_{P_{S2}(x,y)}(\lambda) \cong R_{P_{nCOATING}(x,y)}(\lambda)$ (Eq. (6)), was obtained by using Eq. (7), assuming the reflectance selected from bright and dark areas of the painting with the coating ($R^{white}_{P_{COATING}}(\lambda)$ and $R^{black}_{P_{COATING}}(\lambda)$) and without the coating ($R^{white}_{P_{nCOATING}}(\lambda)$and $R^{black}_{P_{nCOATING}}(\lambda)$), a uniformly varnished surface, and excluding the specular component by including the Saunderson's correction [22,53–55].

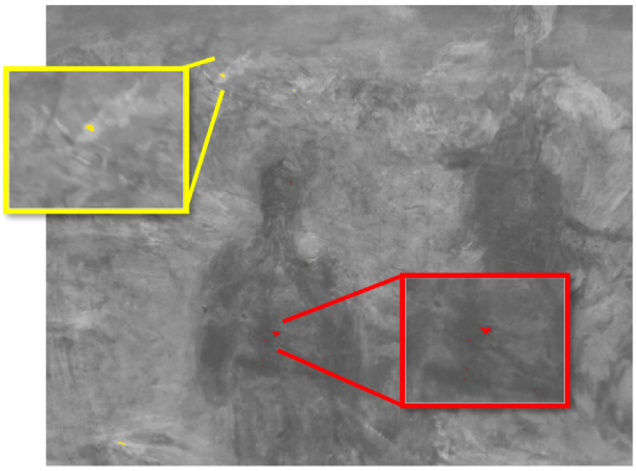

Fig. 3. Grayscale image of Painting 1 without the coating, with the 50 brightest (yellow dots) and darkest (red dots) pixels highlighted (yellow and red inset squares zooms in the selected pixels for better visualization).

$$R_{P_{COATING}(x,y)}(\lambda) = R_V^b(\lambda) + \frac{T^2(\lambda)\,.\,R_P^b(\lambda)}{1 - R_V^b(\lambda)\,.\,R_P^b(\lambda)} \tag{4}$$

$$T(\lambda) = \left[\frac{R^{white}_{P_{COATING}}(\lambda) - R^{black}_{P_{COATING}}(\lambda)}{R^{white}_{P_{nCOATING}}(\lambda) - R^{black}_{P_{nCOATING}}(\lambda)} - R^{black}_{P_{COATING}}(\lambda).\left(R^{white}_{P_{COATING}}(\lambda) - R^{black}_{P_{COATING}}(\lambda)\right)\right]^{\frac{1}{2}} \tag{5}$$

$$R_{P_{nCOATING}(x,y)}(\lambda) = R_P^i(\lambda) + R_P^b(\lambda) \tag{6}$$

$$R_{P_{S2}(x,y)}(\lambda) \cong R_{P_{nCOATING}(x,y)}(\lambda) = \frac{R_{P_{COATING}(x,y)}(\lambda) - R^{black}_{P_{COATING}}(\lambda)}{T(\lambda)^2 + R^{black}_{P_{COATING}}(\lambda).\left(R_{P_{COATING}(x,y)}(\lambda) - R^{black}_{P_{COATING}}(\lambda)\right)} + R^{black}_{Pn_{COATING}}(\lambda) \tag{7}$$

The parameters $R_V^b(\lambda)$, $R_P^i(\lambda)$, and $T(\lambda)$ were estimated using the reflectance selected from bright and dark areas of the painting with the coating ($R^{white}_{P_{COATING}}(\lambda)$ and $R^{black}_{P_{COATING}}(\lambda)$) and without the coating ($R^{white}_{P_{nCOATING}}(\lambda)$and $R^{black}_{P_{nCOATING}}(\lambda)$). To avoid the oversimplification of selecting a single bright or dark pixel possibly associated with a highlight, hot pixel, dead pixel or a noise highly contaminated pixel, the average reflectance of the 50 brightest and darkest independent pixels was estimated and used as the bright and dark reflectance, respectively. These pixels were selected from a grayscale image rendered from the painting's hyperspectral image without the coating, to reduce its possible influence, and spatial coordinates recorded. Fig. 3 represents the grayscale image rendered from the hyperspectral image of Painting 1 without the coating, with the 50 brightest (yellow dots) and darkest (red dots) pixels highlighted [23].

Assuming that the substrate, corresponding to the selected black area, absorbs all the incident light, $R_V^b(\lambda)$ was assumed to be equal to $R^{black}_{P_{COATING}}(\lambda)$, and $R_P^i(\lambda)$ equal to $R^{black}_{P_{nCOATING}}(\lambda)$.

Eq. (8) represents Saunderson's correction applied to all reflectance data to remove the reflection and scattering components at the air-painting interface caused by the illumination/acquisition geometry. In Eq. (8), $i_0 = 0.04$ and $i_2 = 0.6$ were based on the Fresnel coefficients, assuming a varnish with a refractive index of

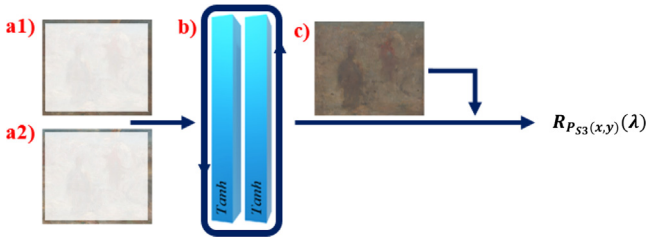

Fig. 4. NN framework devised to virtually remove a painting's coating. a) shows a rendering of the reflectance data used as input to train the NN, corresponding to the W30 area of pixels of the painting (as in Figure 2) with (a1)) and without (a2)) the coating, b) outlines the basic structure of the two layer NN, and c) an image rendered from the reflectance data of a painting with the coating used as input to simulate the virtual removal of the coating. The output was a hyperspectral image of the painting with the reflectance spectra without the influence of the coating - $R_{P_{S3}(x,y)}(\lambda)$.

1.5, and an illumination/acquisition geometry relative to the painting of 45°/0° $R_m(\lambda)$ represents the reflectance with the Saunderson's corrections, and $R_t(\lambda)$ represents the reflectance from the paintings' hyperspectral images [22,53–55].

$$R_m(\lambda) = \frac{(1-i_0).(1-i_2).R_t(\lambda)}{1-i_2 .R_t(\lambda)} \quad (8)$$

3.5.3. Coating removal method 3: neural network (NN)

Fig. 4 outlines the third methodology: a sequential NN that generates a hyperspectral image of a painting without its coating, using as input hyperspectral image of the paintings with the coating.

Consistent with the rationale presented in method 1, the stripe of pixels that surrounded the image of the painting (W30) was used in method 3. Fig. 4 *a1)* and *a2)* represent the pixels of the image from which the reflectance data used to train the NN (Fig. 4 *b)*) was retrieved, with and without the coating, respectively. After training the NN, the hyperspectral image of the painting with the coating was used as input to the NN (Fig. 4 *c)*), resulting in an output of the hyperspectral image of the painting without the coating.

Fig. 4 b), represents the devised sequential NN composed by 2 hidden layers, each with 33 nodes using the hyperbolic tangent activation function (*Tanh*), trained to virtually remove the coating using the inputs provided over 50 complete epochs, assuming the Nesterov Accelerated Adaptive Moment (*nadam*) optimizer. The loss function '*mean squared error*' was used to assess the performance of the NN.

The *Tanh* function provides a better adjustment when considering models that need to predict the output based on the probability of existence, and the *nadam* optimizer, which combines the advantages of the RMSprop, the SGD Moment, and the Nesterov Accelerated Gradient, was used to enhance the efficiency and speed of the NN training.

3.6. Simulating the colors of the images from the hyperspectral image data

Reflectance data from the hyperspectral images was converted into tristimulus values (XYZ) assuming the CIE D65 standard illuminant, and the CIE 2006 LMS cone fundamentals for 10° color-matching functions. Color images were rendered from the XYZ values assuming the sRGB color space [42,43,50,56,57].

Colorimetric analyses were performed in CIECAM16-UCS, a perceptual color space [58], allowing the representation of the perceived amounts of green or red, blue or yellow, and lightness of a color by using the coordinates *a'*, *b'* and *J'*, respectively. Conversions assumed the luminance of the adapting field (L_A) of 20 cd/m^2, the background luminance (Y_b) of 50 cd/m^2, the surround condition set for "average", and the CIE D65 illuminant as the reference white [58–60].

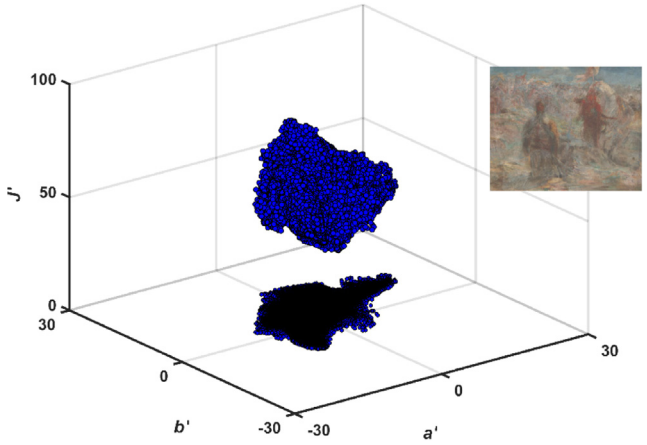

Fig. 5. CIECAM16-UCS color volume estimated from Painting 1 without the coating (represented in the inset). Each coordinate within the color volume represents the color of a pixel from the image of the painting, retrieved from the hyperspectral image. Lower shaded area represents the projection of the color volume in the CIECAM16-UCS (a',b') chromaticity diagram.

Fig. 5 shows the color volume of the CIECAM16-UCS coordinates estimated from the reflectance data of *Painting 1* without the coating. Each coordinate represents a pixel in the painting's image, representing the color perceived by a CIE 2006 observer when viewing *Painting 1* under CIE D65 illumination. All chromaticity coordinates represented in the color volume constitute the color gamut, while the shaded area at the bottom of the figure represents the projection of the color volume in the CIECAM16-UCS (*a',b'*) chromaticity diagram.

3.7. Metrics for evaluating chromatic diversity

Chromatic changes between paintings with and without coating, and paintings without coating and the virtual simulation ($R_{P_{S1}(x,y)}(\lambda)$, $R_{P_{S2}(x,y)}(\lambda)$, and $R_{P_{S3}(x,y)}(\lambda)$), were estimated by comparing the number of just-noticeable different colors (JND) and the chromatic differences.

The JND was assumed to represent the chromatic diversity perceived by an observer when viewing a painting. It was estimated by segmenting the CIECAM16-UCS into cubes of 0.5 units and assuming that all chromaticity coordinates within the same cube were not discernible and counted as one color [61–63]. The JND was estimated by counting the number of non-empty cubes. An increase in the JND was considered to be an increase in the chromatic content of the painting [61,63,64], and vice-versa.

Variations in JND between paintings in two conditions were estimated by computing the ratio between them P_a:P_b, by Eq. (9), where JND_{Pa} and JND_{Pb} represent the JND of the painting after (P_a) and before (P_b) the removal of the coating, respectively:

$$P_a : P_b = \frac{JND_{P_a}}{JND_{P_b}} \quad (9)$$

The chromatic differences between the paintings' color volumes before and after the removal of the coating were estimated by computing the color difference between corresponding pixels using the color difference - $\Delta E'$ - as in Eq. (10) [58].

$$\Delta E' = \sqrt{(J'_b - J'_a)^2 + (a'_b - a'_a)^2 + (b'_b - b'_a)^2} \quad (10)$$

Where *J'*, *a'*, and *b'* represent the CIECAM16-UCS chromaticity coordinates from the color volume of the painting, before (*b*) and

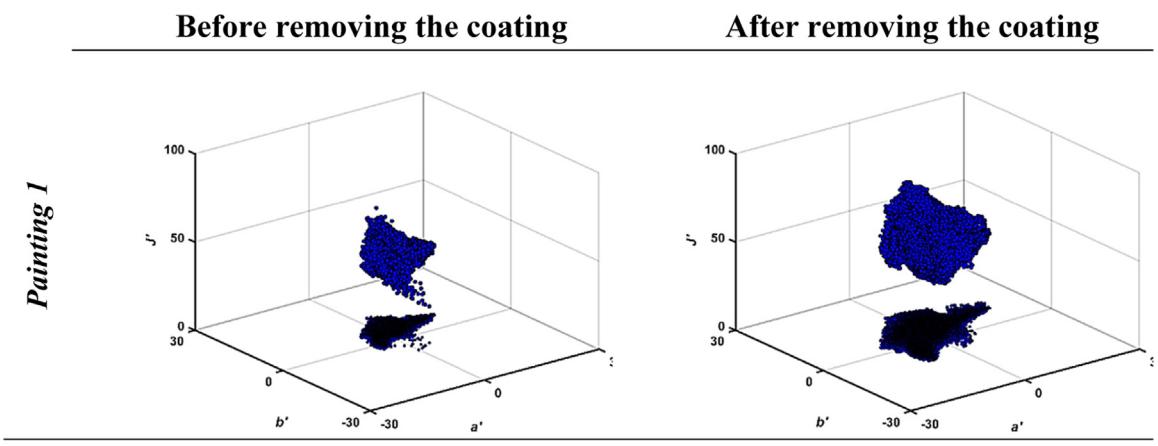

Fig. 6. CIECAM16-UCS color gamut for Painting 1 before (left column) and after (right column) the removal of the coating. Each coordinate within the color volume represents the color of a pixel from the image of the painting, retrieved from the hyperspectral image data. Shaded areas at the bottom of the diagram represent the color gamut projection in the CIECAM16-UCS (a',b') chromaticity diagram.

Table 1
Variation of the JND ($P_a : P_b$) and the average chromatic difference for each painting, as estimated by the ratio represented in Eq. (9) and Eq. (10). $P_a : P_b$ values higher than 1 represent an increase, while lower than 1 represent a decrease from before to after the removal of the painting's coating. Values in brackets represent the standard deviation associated with the average estimated across paintings.

	JND ($P_a : P_b$)		$\Delta E'$	$\Delta E'(a',b')$
	CIECAM16-UCS	CIECAM16- UCS (a',b')	Average (±STD)	Average (±STD)
Painting 1	3,4	2,4	10,4 (±4,4)	2,5 (±2,1)
Painting 2	1,9	1,7	3,7 (±2,2)	1,6 (±0,9)
Painting 3	1,7	1,6	3,7 (±2,3)	1,2 (±0,8)
Painting 4	1.4	1.1	3,0 (±2,0)	1,0 (±0,6)
Painting 5	0,8	1,0	5,6 (±3,9)	2,0 (±1,3)
Average	1,8 (±0,9)	1,6 (±0,5)	5,3 (±2,7)	1,7 (±0,5)

after (a) the removal of the coating. The overall chromatic difference was estimated by averaging the $\Delta E'$ across all pixels.

Estimating changes in the paintings' chromatic diversity upon coating removal will provide information regarding the coating's influence on the visual interpretation of the painting, particularly whether the coating impairs or enhances color perception. This analysis will establish the expected results for simulation methodologies.

4. Results

Results for all paintings are provided in the Supplementary Material.

Fig. 6, represents the CIECAM16-UCS of *Painting 1* before (left) and after (right) the physical removal of the coating. Each coordinate within the color volume represents the color of a pixel computed from the painting's hyperspectral image. An increase in color volume after the coating removal implies an impairing effect of the coating on the visual interpretation of the painting with the coating, as the coating reduces the chromatic diversity available to the observer.

Table 1 represents the variations in the JND and the average chromatic difference between the painting before and after removing the coating (P_a:P_b), as estimated by Eq. (9) and Eq. (10), respectively. All paintings had a ratio P_a:P_b higher than 1 (an increase in the JND), except for *Painting 5* if the J' dimension was ignored.

The average chromatic difference ($\Delta E'$) across all paintings, when considering a', b' and J', was found to be approximately three times greater than when estimating the same quantity ignoring J'.

Fig. 7 represents for *Painting 1* the resulting color gamut of the virtual removal of the coating across the three methods. $\boldsymbol{R_{P_{S1}(x,y)}(\lambda)}$ represents the color gamut (red dots) resulting from the simulation using the average coating of the W30 area, $\boldsymbol{R_{P_{S2}(x,y)}(\lambda)}$ represents the color gamut (green dots) from the simulation using the Kubelka-Munk theory, $\boldsymbol{R_{P_{S3}(x,y)}(\lambda)}$ represents the color gamut (yellow dots) from the simulation using the NN.

The $\boldsymbol{R_{P_{S3}(x,y)}(\lambda)}$ produced a color gamut that better resembled the color gamut of *Painting 1* without the coating, represented in Fig. 5 while $\boldsymbol{R_{P_{S2}(x,y)}(\lambda)}$ showed the higher difference.

Table 2 shows the variation in the JND as the ratio between the JND found for the painting virtually simulated without and physically without the coating, $\boldsymbol{P_{simulated} : P_{original}}$, in CIECAM16-UCS.

Ratios greater than 1 show an increase in the JND in the simulated image of the painting, while <1 show a decrease. On average, variations were higher in $\boldsymbol{R_{P_{S2}(x,y)}(\lambda)}$, whereas variations resulting from the simulations for $\boldsymbol{R_{P_{S1}(x,y)}(\lambda)}$ and $\boldsymbol{R_{P_{S3}(x,y)}(\lambda)}$ were closer to the real painting.

Table 3 represents the average color difference between the original painting without the coating and the simulations of the virtual removal of the coating in CIECAM16-UCS. The highest color difference averaged across analyzed paintings was found when using the Kubelka-Munk theory while the simulation using the NN achieved the lowest average color difference.

Fig. 8 shows sRGB renderings of the reflectance data retrieved from the original *Painting 1* without the coating ($\boldsymbol{R_{P_{nCOATING}}(\lambda)}$) and the three simulations of the removal of the coating ($\boldsymbol{R_{P_{S1}(x,y)}(\lambda)}$, $\boldsymbol{R_{P_{S2}(x,y)}(\lambda)}$, *and* $\boldsymbol{R_{P_{S3}(x,y)}(\lambda)}$).

5. Discussion

The removal of a painting's coating changes the observer's chromatic perception when viewing it. The distribution of the chromaticity coordinates estimated before and after coating removal was found to increase with coating removal, showing an increased color volume and a shift towards higher J' values, except for *Painting 5*. *Paintings 1* through *4* showed average variations of the JND

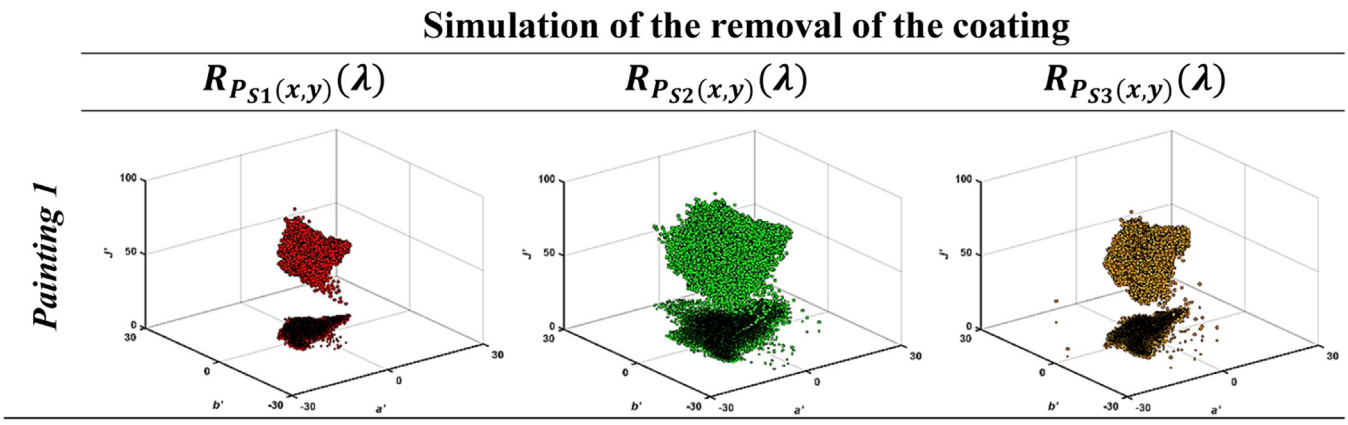

Fig. 7. CIECAM16-UCS color gamut resulting from the virtual removal of the coating for Painting 1. $\boldsymbol{R_{P_{S1}(x,y)}(\lambda)}$ (red dots) represent the simulation using the average coating, $\boldsymbol{R_{P_{S2}(x,y)}(\lambda)}$ (green dots) represent the simulations using Kubelka-Munk theory and $\boldsymbol{R_{P_{S3}(x,y)}(\lambda)}$ (yellow dots) represent the simulation using the NN. Shadowed area represents the color gamut projection in the CIECAM16-UCS (a',b') chromaticity diagram. Fig. 5 represents the color volume obtained after the removal of the painting's coating, which serves as reference for comparison.

Table 2
Variation in the JND as the ratio between the JND from the painting simulated for the virtual removal of the coating and the JND for the original painting without the coating, $\boldsymbol{P_{simulated} : P_{original}}$, in CIECAM16-UCS and CIECAM16-UCS (a', b'). Values in brackets represent the standard deviation associated with the average estimated across analyzed paintings.

JND ($P_{simulated} : P_{original}$)				
Painting	CIECAM16-UCS	$R_{P_{S1}(x,y)}(\lambda)$	$R_{P_{S2}(x,y)}(\lambda)$	$R_{P_{S3}(x,y)}(\lambda)$
1	*(J', a',b')*	0,4	2,0	0,8
	(a',b')	0,6	1,9	0,9
2	*(J', a',b')*	0,5	3,9	0,8
	(a',b')	0,6	3,8	0,9
3	*(J', a',b')*	0,6	1,7	0,6
	(a',b')	0,6	1,4	1,2
4	*(J', a',b')*	0,6	2,6	0,5
	(a',b')	0,8	1,7	0,8
5	*(J', a',b')*	1,1	4,9	0,6
	(a',b')	0,9	3,3	0,9
Average	*(J', a',b')*	0,7 (±0,2)	3,0 (±1,2)	0,7 (±0,1)
	(a',b')	0,7 (±0,1)	2,4 (±1,0)	0,9 (±0,1)

Table 3
shows the average color difference ($\Delta \boldsymbol{E}'$) between the original paintings without the coating and the paintings obtained from the virtual simulations of the removal of the coating, in CIECAM16-UCS and CIECAM16-UCS (a',b'). Values in brackets represent the standard deviation associated with the average estimated across the analyzed paintings.

Average color difference between the original painting without coating and the painting simulated without the coating ($\Delta E'$)				
Painting	CIECAM16-UCS	$R_{P_{S1}(x,y)}(\lambda)$	$R_{P_{S2}(x,y)}(\lambda)$	$R_{P_{S3}(x,y)}(\lambda)$
1	*(J', a',b')*	4,4 (±2,5)	9,1 (±4,1)	3,5 (±2,2)
	(a',b')	2,1 (±1,5)	2,1 (±1,4)	1,4 (±0,9)
2	*(J', a',b')*	3,4 (±2,2)	4,7 (±3,8)	2,0 (±1,3)
	(a',b')	1,1 (±0,7)	2,4 (±2,1)	0,9 (±0,6)
3	*(J', a',b')*	3,4 (±2,2)	6,1 (±3,1)	2,7 (±1,9)
	(a',b')	1,2 (±0,7)	2,1 (±1,0)	1,1 (±0,6)
4	*(J', a',b')*	2,9 (±1,7)	3,5 (±1,9)	2,0 (±1,4)
	(a',b')	1,0 (±0,6)	2,1 (±1,3)	0,9 (±0,6)
5	*(J', a',b')*	5,6 (±3,6)	19,4 (±9,5)	2,6 (±1,6)
	(a',b')	2,0 (±1,4)	9,7 (±4,6)	1,4 (±0,9)
Average	*(J', a',b')*	3,9 (±1,0)	8,6 (±5,7)	2,6 (±0,5)
	(a',b')	1,5 (±0,5)	3,7 (±3,0)	1,1 (±0,2)

greater than 1 with coating removal, implying increased chromatic variability and higher saturation.

Painting 5 exhibited a unique pattern, as removing the coating resulted in a contraction of the color volume and a reduction in the JND. The cracks found in *Painting 5*'s coating increased reflection at the air-coating interface and affected light absorption and transmission [65] increasing the reflected light measured by the HIS. Removing the coating eliminated these cracks, leading to a lower estimated color volume and reduced JND. Although similar cracks were found in all paintings, *Painting 5* had the most pronounced effect. Since no analysis was performed on the overall degree of degradation of the coating, it is possible that the coating over this painting was still saturating the colors while fulfilling its protective function.

The estimated color differences between the painting with coating and the simulated removal of the coating may be directly correlated with the perceptual differences perceived by the CIE2006 standard observer when observing the paintings. A $\Delta E > 1.0$ was assumed as the JND threshold, as paintings were considered complex stimuli, increasing the magnitude of the JND found for sim-

Fig. 8. sRGB renderings of the reflectance data retrieved from the original Painting 1 without the coating ($\boldsymbol{R}_{P_{nCOATING}}(\boldsymbol{\lambda})$) and the three simulations of the virtual removal of the coating ($\boldsymbol{R}_{P_{S1}(x,y)}(\boldsymbol{\lambda})$, $\boldsymbol{R}_{P_{S2}(x,y)}(\boldsymbol{\lambda})$, and $\boldsymbol{R}_{P_{S3}(x,y)}(\boldsymbol{\lambda})$) for simulation methods 1, 2 and 3, respectively. These images do not represent true colors and are intended only as visual representations of the simulation results. Quantifications of the simulation results are represented in Table 2 and Table 3.

ple and uniform stimuli of about 0.5 units [66]. When comparing color differences between the paintings without the coating and their simulated versions, the average color differences were found to be higher than 1, indicating that the simulated paintings were perceptually distinct from the original paintings without the coating.

The Kubelka-Munk two-constant theory, $\boldsymbol{R}_{P_{S2}(x,y)}(\boldsymbol{\lambda})$, generated simulations with the highest color differences compared to the original paintings without the coating, approximately 9 and 4 times higher than the unitary reference. These simulations showed an expanded color volume as inferred from the JND ratios, indicating the presence of more saturated colors and colors with a higher range of J'values. Such color differences were unexpected when compared with other methodologies. One explanation could be the existence of debris, dirt, and an aged coating with several cracks that could impair the Kubelka-Munk model when simulating the transmittance of the coating, which assumed a uniform layer of clear coating.

No analysis was performed to determine the refractive index of the aged varnish. However, a refractive index of 1.5 was assumed when required, based on the typical refractive index of commonly used varnishes. All computations were performed without knowing the exact composition of the coatings. Nevertheless, using spectral data from the paintings with and without coating was sufficient to obtain these results.

When estimating the average reflectance of the 50 brightest and darkest pixels, individual pixels were selected instead of broader areas to ensure that lighter or darker pixels were considered but then averaged to minimize the influence of signal noise from individual pixels. However, some paintings did not contain purely white or black substrate pixels, limiting the applicability of the Kubelka-Munk theory. To overcome this limitation, a new simulation was tested with fewer than 50 of the darkest or brightest pixels. The simulations produced worse results, demonstrating that using single pixels or a very small number of pixels should be avoided.

Additionally, methodology $\boldsymbol{R}_{P_{S1}(x,y)}(\boldsymbol{\lambda})$ could not simulate the removal of the coating as good as methodology $\boldsymbol{R}_{P_{S3}(x,y)}(\boldsymbol{\lambda})$, as using the average spectral reflectance estimated across all pixels of the hyperspectral image, disregarding local non uniformities, debris or dust that may vary across painting's surface, hindered the simulation of the paintings without the coating. To support this statement, local averages of the reflectance spectra were used when simulating the removal of the coating, starting with pixelwise simulation to ever increasing clusters of pixels. Using Eq. (2), the best results were found when the simulation was estimated pixelwise, revealing good results but unpractical and not useful, as it would require the entire painting with and without the coating to extract the reflectance spectra at the pixel level, making the simulation redundant. If increasing clusters of pixels were considered as the local average reflectance, the color difference between the simulation and the original without the coating would be below 1 unit in CIECAM16-UCS only if a cluster of 5 × 5 pixels was considered. Higher clusters of pixels produced a result worse than methodology $\boldsymbol{R}_{P_{S3}(x,y)}(\boldsymbol{\lambda})$. Nevertheless, having the average spectral reflectance of a cluster of 5 × 5 pixels across the entire painting would require access to the complete hyperspectral image of the painting with and without the coating, also making the simulation redundant. If methodology $\boldsymbol{R}_{P_{S1}(x,y)}(\boldsymbol{\lambda})$ used the same pixel area (W30) as methodology $\boldsymbol{R}_{P_{S3}(x,y)}(\boldsymbol{\lambda})$, results would still be worse than those obtained with methodology $\boldsymbol{R}_{P_{S3}(x,y)}(\boldsymbol{\lambda})$.

Methodology $\boldsymbol{R}_{P_{S3}(x,y)}(\boldsymbol{\lambda})$, considering the area of pixels that would be hidden underneath the painting's frame (W30), provided the simulated image without the coating that was closest to the original in terms of the JND and the $\Delta E'$. When ignoring the J' coordinate, color differences were even smaller, making the simulated and original paintings very close in chromatic and visual terms.

The impact of cross training the NN with one painting and testing the coating removal simulation with another painting was also tested using methodology $\boldsymbol{R}_{P_{S3}(x,y)}(\boldsymbol{\lambda})$, resulting in an increase in the average color differences across paintings to around 4 $\boldsymbol{\Delta E'}$, indicating that the simulation improves when the NN is trained with pixels from the painting that will be used in the simulation. Cross-training the NN impairs the results obtained, but they are still closer to and better than other methodologies tested.

Despite the simple structure of the NN used in methodology $\boldsymbol{R}_{P_{S3}(x,y)}(\boldsymbol{\lambda})$, and the use of peripheral pixels in training (around 10 % of the painting's pixels, typically covered by the painting's frame), the simulations of the removal of the coating were closer to the original. Using only surrounding pixels did not seem to impact greatly the simulation, as in methodology $\boldsymbol{R}_{P_{S1}(x,y)}(\boldsymbol{\lambda})$, despite the fact that peripheral pixels did not represent all the spatial variations in the thickness of the coating, the existence of dirt on or under the coating, and the exposure to other external factors (as the area of the painting these pixels represent was, generally, under a frame). The complex process of removing the coating from the paintings, described in the Supplementary Materials, revealed the nonuniformity and spatial variation of the coating, supporting the need for a methodology that could consider the painting with and without the coating across its surface. Analyzing the surrounding area of the painting that was under the frame enabled just that. These are common artefacts that exist in real cases of restoration and a limitation in the performance of some of the methodologies presented. Nevertheless, the methodologies evaluated are independent of the painting technique, pigments, binders, composition, substrate, among others. Additionally, these intrinsic properties of each painting could not be isolated in this study to determine their influence on the results. Only the spectral changes when removing the coating were required, and only one model ($\boldsymbol{R}_{P_{S2}(x,y)}(\boldsymbol{\lambda})$) required assumptions regarding the coating type.

6. Conclusion

Removing the paintings' coating resulted in changes in their color perception, demonstrated by an increase in their chromatic diversity and color saturation. Nevertheless, caution is needed when considering simulations of the coating removal, as accurate predictions require a comprehensive understanding of the coating's properties, including its condition, distribution, uniformity, and exposure to external factors. In the absence of such data, the use of models as the Kubelka-Munk theory may be impaired.

The NN generated simulations that closely resembled the original painting without the coating, a simulation that was improved if the J' (lightness) color coordinate was not considered. Despite its simple structure and use of only 10 % of the painting's hyperspectral image data, the NN could simulate accurately the removal of the coating. The NN method was not only the most accurate but also achieved the best result with minimal visible intervention by requiring intervention only in the area that sits under the painting's frame.

These results show the suitability of three methods for simulating the removal of the coating from paintings based on the spectral reflectance of the paintings, with better results when using a NN to perform the simulation.

Simulating the coating removal with minimal intervention, as achieved by the NN method, provides a valuable tool for conservators to devise conservation plans that preserve the integrity of the original artwork.

Funding

This study was supported by the Portuguese Foundation for Science and Technology (FCT) under the scope of the strategic funding of UIDB/04650/2020 and by PhD Scholarship UI/BD/152222/2021 (DOI: https://doi.org/10.54499/UI/BD/152222/2021)

References

[1] L. Simonot, M. Elias, Color change due to a varnish layer, Color Res. Appl. 29 (3) (2004) 196–204, doi:10.1002/col.20008.
[2] C. Montagner, J.M.M. Linhares, M. Vilarigues, M.J. Melo, S.M.C. Nascimento, Supporting history of art with colorimetry: the paintings of Amadeo de Souza-Cardoso, Color Res. Appl. 43 (3) (2018) 304–310, doi:10.1002/col.22189.
[3] R.S. Berns, E.R. de la Rie, The effect of the refractive index of a varnish on the appearance of oil paintings, Stud. Conserv. 48 (4) (2003) 251–262, doi:10.1179/sic.2003.48.4.251.
[4] H. Pasco, A. Lesaine, A. Cerasuolo, C. Boissière, P. Walter, C. Sanchez, L. De Viguerie, M. Faustini, In situ infrared and UV–Vis ellipsometries to probe the varnish ageing and swelling of G. Bellini *"transfiguration."*, Adv. Mater. Interfaces 11 (6) (2024) 2300563, doi:10.1002/admi.202300563.
[5] G. Trumpy, D. Conover, L. Simonot, M. Thoury, M. Picollo, J.K. Delaney, Experimental study on merits of virtual cleaning of paintings with aged varnish, Opt. Express 23 (26) (2015) 33836, doi:10.1364/OE.23.033836.
[6] G. Latour, M. Elias, J.-M. Frigerio, Determination of the absorption and scattering coefficients of pigments: application to the identification of the components of pigment mixtures, Appl. Spectrosc. 63 (6) (2009) 604–610, doi:10.1366/000370209788559719.
[7] E.R. de la Rie, E.R. de la Rie, The influence of varnishes on the appearance of paintings, Stud. Conserv. 32 (1) (1987) 1, doi:10.2307/1506186.
[8] M. Elias, N. Mas, P. Cotte, Review of several optical non-destructive analyses of an easel painting. Complementarity and crosschecking of the results, J. Cult. Herit. 12 (4) (2011) 335–345, doi:10.1016/j.culher.2011.05.006.
[9] M. Barni, F. Bartolini, V. Cappellini, Image processing for virtual restoration of artworks, IEEE Multimed. 7 (2) (2000) 34–37, doi:10.1109/93.848424.
[10] L. Masschelein-Kleiner, Ancient Binding Media, Varnishes and Adhesives, 2nd ed., ICCROM, 1995.
[11] N. De Keyser, F. Broers, F. Vanmeert, S. De Meyer, F. Gabrieli, E. Hermens, G. Van der Snickt, K. Janssens, K. Keune, Reviving degraded colors of yellow flowers in 17th century still life paintings with macro- and microscale chemical imaging, Sci. Adv. 8 (23) (2022) eabn6344, doi:10.1126/sciadv.abn6344.
[12] Dauvergne, C. (2024, April 30). *Retour en salle de "La Liberté guidant le peuple" restaurée*. Espace presse du musée du Louvre. https://presse.louvre.fr/?p=1063000217991
[13] S. Berns, Rejuvenating the appearance of cultural heritage using color and imaging science techniques, in: AIC Colour 05 - 10th Congress of the International Colour Association, 2005, p. 6.
[14] M. Elias, P. Cotte, Multispectral camera and radiative transfer equation used to depict Leonardo's sfumato in Mona Lisa, Appl. Opt. 47 (12) (2008) 2146, doi:10.1364/AO.47.002146.
[15] M. Pappas, I. Pitas, Digital color restoration of old paintings, IEEE Trans. Image Process. 9 (2) (2000) 291–294, doi:10.1109/83.821745.
[16] F. Daniel, A. Mounier, J. Pérez-Arantegui, C. Pardos, N. Prieto-Taboada, S. Fdez-Ortiz de Vallejuelo, K. Castro, Comparison between non-invasive methods used on paintings by Goya and his contemporaries: hyperspectral imaging vs. point-by-point spectroscopic analysis, Anal. Bioanal. Chem. 409 (16) (2017) 4047–4056, doi:10.1007/s00216-017-0351-5.
[17] J. Linhares, L. Cardeira, A. Bailão, R. Pastilha, S. Nascimento, Chromatic changes in paintings of Adriano de Sousa Lopes after the removal of aged varnish, Conserv. Patrim. 34 (2020) 50–64, doi:10.14568/cp2018064.
[18] M. Picollo, A. Casini, C. Cucci, L. Stefani, R. Jiménez-Garnica, L. Fuster-López, Documentation and analysis of some Picasso's paintings by using hyperspectral imaging technique to support their conservation and stylistic matters, IOP Conf. Ser.: Mater. Sci. Eng. 949 (1) (2020) 012023, doi:10.1088/1757-899X/949/1/012023.
[19] M. Thoury, M. Elias, J.M. Frigerio, C. Barthou, Nondestructive varnish identification by ultraviolet fluorescence spectroscopy, Appl. Spectrosc. 61 (12) (2007) 1275–1282, doi:10.1366/000370207783292064.
[20] M. Spring, C. Ricci, D.A. Peggie, S.G. Kazarian, ATR-FTIR imaging for the analysis of organic materials in paint cross sections: case studies on paint samples from the National Gallery, London, Anal. Bioanal. Chem. 392 (1–2) (2008) 37–45, doi:10.1007/s00216-008-2092-y.
[21] H.S. Shah, F.W. Billmeyer, Kubelka-munk analysis of absorptance in the presence of scattering, including surface-reflection correction to transmittance, Color Res. Appl. 10 (1) (1985) 26–31, doi:10.1002/col.5080100107.
[22] H.G. Völz, Industrial Color Testing, 1st ed., Wiley, 2001, doi:10.1002/3527600485.
[23] E. Kirchner, I. Van Der Lans, F. Ligterink, E. Hendriks, J. Delaney, Digitally reconstructing Van Gogh's *field with Irises near Arles* . Part 1: varnish, Color Res. Appl. 43 (2) (2018) 150–157, doi:10.1002/col.22162.
[24] P. Kubelka, New contributions to the optics of intensely light-scattering materials part II: nonhomogeneous layers, J. Opt. Soc. Am. 44 (4) (1954) 330, doi:10.1364/JOSA.44.000330.
[25] R.Y. Choi, A.S. Coyner, J. Kalpathy-Cramer, M.F. Chiang, J.P. Campbell, Introduction to machine learning, neural networks, and deep learning, Transl. Vis. Sci. Technol. 9 (2) (2020) 14, doi:10.1167/tvst.9.2.14.
[26] J. Feng, S. Lu, Performance analysis of various activation functions in artificial neural networks, J. Phys.: Conf. Ser. 1237 (2) (2019) 022030, doi:10.1088/1742-6596/1237/2/022030.
[27] T.P. Lillicrap, A. Santoro, L. Marris, C.J. Akerman, G. Hinton, Backpropagation and the brain, Nat. Rev. Neurosci. 21 (6) (2020) 335–346, doi:10.1038/s41583-020-0277-3.
[28] R. Zaheer, H. Shaziya, A study of the optimization algorithms in deep learning, in: 2019 Third International Conference on Inventive Systems and Control (ICISC), 2019, pp. 536–539, doi:10.1109/ICISC44355.2019.9036442.
[29] R. Yamashita, M. Nishio, R.K.G. Do, K. Togashi, Convolutional neural networks: an overview and application in radiology, Insights Imaging 9 (4) (2018) 611–629, doi:10.1007/s13244-018-0639-9.
[30] P.Y. Simard, D. Steinkraus, J.C. Platt, Best practices for convolutional neural networks applied to visual document analysis, in: Seventh International Con-

ference on Document Analysis and Recognition, 2003. Proceedings, 1, 2003, pp. 958–963, doi:10.1109/ICDAR.2003.1227801.
[31] N. Strisciuglio, M. Lopez-Antequera, N. Petkov, Enhanced robustness of convolutional networks with a push–pull inhibition layer, Neural Comput. Appl. 32 (24) (2020) 17957–17971, doi:10.1007/s00521-020-04751-8.
[32] M. Maali Amiri, D.W. Messinger, Virtual cleaning of works of art using deep convolutional neural networks, Herit. Sci. 9 (1) (2021) 94, doi:10.1186/s40494-021-00567-4.
[33] A. Flachot, K.R. Gegenfurtner, Processing of chromatic information in a deep convolutional neural network, J. Opt. Soc. Am. A 35 (4) (2018) B334, doi:10.1364/JOSAA.35.00B334.
[34] A. Flachot, A. Akbarinia, H.H. Schütt, R.W. Fleming, F.A. Wichmann, K.R. Gegenfurtner, Deep neural models for color classification and color constancy, J. Vis. 22 (4) (2022) 17, doi:10.1167/jov.22.4.17.
[35] J. Romero, L. Gómez-Robledo, J. Nieves, Computational color analysis of paintings for different artists of the XVI and XVII centuries, Color Res. Appl. 43 (3) (2018) 296–303, doi:10.1002/col.22211.
[36] P. Cotte, D. Dupraz, Spectral imaging of Leonardo Da Vinci's Mona Lisa: a true color smile without the influence of aged varnish, Conf. Colour Graph. Imaging Vis. 3 (7) (2006), doi:10.2352/CGIV.2006.3.1.art00064.
[37] C.B. Wilda, A. Burnstock, K. Suhling, F. Mattioli Della Rocca, R.K. Henderson, J. Nedbal, Visualising varnish removal for conservation of paintings by fluorescence lifetime imaging (FLIM), Herit. Sci. 11 (1) (2023) 127, doi:10.1186/s40494-023-00957-w.
[38] R.S. Berns, L. Taplin, F.H. Imai, E. Day, D.C. Day, Spectral imaging of Matisse's pot of geraniums: a case study, in: The Eleventh Color Imaging Conference: Color Science and Engineering Systems, Technologies, Applications, CIC 2003, November 3, 2003, Scottsdale, Arizona, USA, 2003, p. 5.
[39] A. Casini, M. Bacci, C. Cucci, F. Lotti, S. Porcinai, M. Picollo, B. Radicati, M. Poggesi, L. Stefani, Fiber Optic Reflectance Spectroscopy and Hyper-Spectral Image Spectroscopy: Two Integrated Techniques for the Study of the Madonna dei Fusi, R. Salimbeni, L. Pezzati (Eds.), 2005, doi:10.1117/12.611500.
[40] A. Cosentino, Multispectral imaging system using 12 interference filters for mapping pigments, Conserv. Patrim. 21 (2015) 25–38, doi:10.14568/cp2015005.
[41] P.D. Pinto, J.M.M. Linhares, S.M.C. Nascimento, Correlated color temperature preferred by observers for illumination of artistic paintings, J. Opt. Soc. Am. A 25 (3) (2008) 623, doi:10.1364/JOSAA.25.000623.
[42] J.M. Maciel Linhares, P.D. Araújo Pinto, S.M. Cardoso Nascimento, Color rendering of art paintings under CIE illuminants for normal and color deficient observers, J. Opt. Soc. Am. A 26 (7) (2009) 1668, doi:10.1364/JOSAA.26.001668.
[43] S.M.C. Nascimento, J.M.M. Linhares, C. Montagner, C.A.R. João, K. Amano, C. Alfaro, A. Bailão, The colors of paintings and viewers' preferences, Vis. Res. 130 (2017) 76–84, doi:10.1016/j.visres.2016.11.006.
[44] J. Suomalainen, R.A. Oliveira, T. Hakala, N. Koivumäki, L. Markelin, R. Näsi, E. Honkavaara, Direct reflectance transformation methodology for drone-based hyperspectral imaging, Remote Sens. Environ. 266 (2021) 112691, doi:10.1016/j.rse.2021.112691.
[45] M. Bacci, C. Cucci, A. Mencaglia, A. Mignani, Innovative sensors for environmental monitoring in museums, Sensors 8 (3) (2008) 1984–2005, doi:10.3390/s8031984.
[46] C. Stavroudis, Sorting out surfactants, WAAC Newsl. 31 (1) (2009) 18–21.
[47] P.D. Pinto, P.E.R. Felgueiras, J.M.M. Linhares, S.M.C. Nascimento, Chromatic effects of metamers of D65 on art paintings: effects of illuminants on paintings, Ophthalmic Physiol. Opt. 30 (5) (2010) 632–637, doi:10.1111/j.1475-1313.2010.00726.x.
[48] S.M.C. Nascimento, O. Masuda, Best lighting for visual appreciation of artistic paintings—experiments with real paintings and real illumination, J. Opt. Soc. Am. A 31 (4) (2014) A214, doi:10.1364/JOSAA.31.00A214.
[49] P.D. Pinto, J.M.M. Linhares, J.A. Carvalhal, S.M.C. Nascimento, Psychophysical estimation of the best illumination for appreciation of Renaissance paintings, Vis. Neurosci. 23 (3–4) (2006) 669–674, doi:10.1017/S0952523806233340.
[50] J.M.M. Linhares, J.A.R. Monteiro, A. Bailão, L. Cardeira, T. Kondo, S. Nakauchi, M. Picollo, C. Cucci, A. Casini, L. Stefani, S.M.C. Nascimento, How good are RGB cameras retrieving colors of natural scenes and paintings? - a study based on hyperspectral imaging, Sensors 20 (21) (2020) 6242, doi:10.3390/s20216242.
[51] D.H. Foster, K. Amano, Hyperspectral imaging in color vision research: tutorial, J. Opt. Soc. Am. A 36 (4) (2019) 606, doi:10.1364/JOSAA.36.000606.
[52] S. Murugesan, Medical image registration: a matlab based approach, Int. J. Sci. Res. Comput. Sci. Eng. Inf. Technol. 2 (2017) 29–34.
[53] Y. Okumura, Developing a Spectral and Colorimetric Database of Artist Paint Materials, Center for Imaging Science (COS), 2005 https://repository.rit.edu/theses/4892.
[54] U. Hempelmann, 5. Saunderson correction: how surfaces influence the outcome of reflectance measurements, in: P. Gabel, S. Gauss, U. Hempelmann, R. Henning, H.-J. Kremitzl, S. Weixel, G. Wilker, M. Binder, W. Franz (Eds.), Colour Technology of Coatings, Vincentz Network, 2019, pp. 151–156, doi:10.1515/9783748600282-021.
[55] A. García-Valenzuela, F.L.S. Cuppo, J.A. Olivares, An assessment of Saunderson corrections to the diffuse reflectance of paint films, J. Phys.: Conf. Ser. 274 (2011) 012125, doi:10.1088/1742-6596/274/1/012125.
[56] A. Stockman, A.T. Rider, Formulae for generating standard and individual human cone spectral sensitivities, Color Res. Appl. 48 (2023), doi:10.1002/col.22879.
[57] A. Stockman, Cone fundamentals and CIE standards, Curr. Opin. Behav. Sci. 30 (2019) 87–93, doi:10.1016/j.cobeha.2019.06.005.
[58] C. Li, Z. Li, Z. Wang, Y. Xu, M.R. Luo, G. Cui, M. Melgosa, M.H. Brill, M. Pointer, Comprehensive color solutions: CAM16, CAT16, and CAM16-UCS, Color Res. Appl. 42 (6) (2017) 703–718, doi:10.1002/col.22131.
[59] M.R. Luo, G. Cui, C. Li, Uniform colour spaces based on CIECAM02 colour appearance model, Color Res. Appl. 31 (4) (2006) 320–330, doi:10.1002/col.20227.
[60] F. Schiller, K.R. Gegenfurtner, Perception of saturation in natural scenes, J. Opt. Soc. Am. A 33 (3) (2016) A194, doi:10.1364/JOSAA.33.00A194.
[61] Rolf G. Kuehni, How many object colors can we distinguish? Color Res. Appl. 41 (5) (2015) 439–444, doi:10.1002/col.22063.
[62] M.R. Pointer, G.G. Attridge, The number of discernible colours, Color Res. Appl. 23 (1) (1998) 52–54, doi:10.1002/(SICI)1520-6378(199802)23:1(52::AIDCOL8)3.0.CO;2-2.
[63] J.M.M. Linhares, P.D. Pinto, S.M.C. Nascimento, The number of discernible colors in natural scenes, J. Opt. Soc. Am. A 25 (12) (2008) 2918, doi:10.1364/JOSAA.25.002918.
[64] K. Masaoka, R.S. Berns, M.D. Fairchild, F. Moghareh Abed, Number of discernible object colors is a conundrum, J. Opt. Soc. Am. A 30 (2) (2013) 264, doi:10.1364/josaa.30.000264.
[65] J. Flores, Entropy signature for crack networks in old paintings: saturation prospectus, Entropy 20 (10) (2018) 772, doi:10.3390/e20100772.
[66] M. Huang, G. Cui, M. Melgosa, M. Sánchez-Marañón, C. Li, M.R. Luo, H. Liu, Power functions improving the performance of color-difference formulas, Opt. Express 23 (1) (2015) 597, doi:10.1364/OE.23.000597.